PAPER

Ultralong H₂V₃O₈ nanowire bundles as a promising cathode for lithium batteries†

Qinyou An,[a] Jinzhi Sheng,[a] Xu Xu,[a] Qiulong Wei,[a] Yaqin Zhu,[b] Chunhua Han,*[a] Chaojiang Niu[a] and Liqiang Mai*[a]

Ultralong H₂V₃O₈ nanowire bundles with length up to hundreds of micrometers were successfully synthesized by a facile hydrothermal approach. The nanowire bundles exhibit a high specific discharge capacity of 325.7 mA h g⁻¹ at 50 mA g⁻¹. While the current density is up to 2000 mA g⁻¹, the initial specific discharge capacities of a H₂V₃O₈ nanowires cathode can reach 121.1 mA h g⁻¹ with a capacity fading of only 0.0425% per cycle for 300 cycles. Electrical transport of a single nanowire is also recorded *in situ* to detect the evolution of the nanowire during annealing. The conductivity of H₂V₃O₈ nanowire has an increase of three orders of magnitude compared to that of the dehydrated nanowire. The excellent electrochemical performance of H₂V₃O₈ nanowire bundles results from high conductivity and good structural stability. This work demonstrates that H₂V₃O₈ nanowire bundles are a promising cathode material for lithium batteries.

Introduction

With the rapid depletion of world oil reserves, constant emergence of related hazards, and wide applications from advanced portable electronic devices to electric vehicles (EVs) and smart grids, the demand for lithium storage device with high energy and power densities is increasing continuously.[1–5] Indeed, lithium batteries have achieved a leading role in the consumer electronics market with further improvements in terms of energy and power densities. However, there are still requirements for making these systems suitable for application in the electric vehicle.[4–6] In order to increase the high-rate capability and cycle life, many efforts have been made, such as the introduction of electronically conductive phases or the fabrication of unique nanoarchitectures.[6–10] Due to the high electrode–electrolyte contact area, fast Li⁺ diffusion and good strain release, one-dimensional nanomaterials have received great attention in lithium batteries.[9,11]

Vanadium oxides are among the best cathode materials for rechargeable lithium batteries, due to both their large specific capacity and abundant sources.[12–15] However, the development of vanadium oxide electrodes in lithium batteries has been limited by their poor structural stability, low electronic conductivity and slow electrochemical kinetics.[16–18] In particular, H₂V₃O₈ is an intermediate phase in which the ratio of V⁴⁺/V⁵⁺ is 1/2, which would account for a larger theoretical capacity and better resistance to oxidation in air than the metastable VO₂.[19] Compared to V₂O₅, H₂V₃O₈ has a higher electronic conductivity arising from the mixed-valence of V⁴⁺/V⁵⁺.[19,20] In recent years, one-dimensional H₂V₃O₈ nanostructures have been successfully fabricated by a variety of methods and the electrochemical kinetics is indeed improved.[20–23] Nevertheless, it still remains a big challenge to obtain long-term cycling stability during subsequent rapid lithium insertion–extraction processes.[24] Here, we report a facile hydrothermal method to synthesize H₂V₃O₈ nanowires, and the electrical transport properties of a single nanowire are investigated. The H₂V₃O₈ nanowire cathode shows excellent high rate performance and good cycle stability.

[a] *State Key Laboratory of Advanced Technology for Materials Synthesis and Processing, WUT-Harvard Joint Nano Key Laboratory, Wuhan University of Technology, Wuhan, 430070, P. R. China. E-mail: mlq518@whut.edu.cn, hch5927@whut.edu.cn; Fax: +86-027-87644867; Tel: +86-027-87467595*

[b] *Shanghai Institute of Ceramics, Chinese Academy of Sciences, Shanghai, 200050, P. R. China*

Experimental section

Sample preparation

The synthesis route of ultralong H₂V₃O₈ nanowire bundles was modified from our previous works.[24] Basically, vanadium oxide nanowires were successfully prepared by hydrothermal reaction using V₂O₅ sol. Briefly, 1.3 mmol as-prepared V₂O₅ sol, 3.6 μL aniline, and 0.04 g poly(ethylene glycol) (PEG-4000) were mixed by stirring and then transferred into a Telfon-lined stainless steel autoclave and kept at 180 °C for 2 days. The products were

collected and washed repeatedly with deionized water and ethanol, and finally dried at 80 °C for 12 h in air to obtain the ultralong $H_2V_3O_8$ nanowire bundles. In addition, the resultant $H_2V_3O_8$ nanowire bundles were annealed at 400 °C for 3 h in N_2 to obtain V_3O_7 nanowires as a control sample.

Material characterization

X-ray diffraction (XRD) measurements were performed to investigate the crystallographic information using a D/MAX-III X-ray diffractometer with graphite-monochromatized Cu Kα radiation. Thermogravimetry/differential scanning calorimetry (TG/DSC) was performed using a Netzsch STA 449C simultaneous thermal analyzer at a heating rate of 10 °C min^{-1} in N_2. Field emission scanning electron microscopy (FESEM) images were collected with a Hitachi S-4800. Transmission electron microscopy (TEM) and high-resolution transmission electron microscopy (HRTEM) images were recorded by using a JEM-2100F microscope.

Electrochemical measurements

Electrodes were fabricated using a mixture of the nanowires, acetylene black, and PTFE (polytetrafluoroethylene) in a 70 : 20 : 10 weight ratio as the cathode. The thickness of both the electrodes was 30 μm. The electrochemical properties of the electrodes were measured using R2025 coin-type cells in a glove box filled with pure argon gas, while using a lithium pellet as the anode and a 1 M solution of $LiPF_6$ in ethylene carbonate (EC)/dimethyl carbonate (DMC) as the electrolyte. Galvanostatic measurements of the cells were carried out over the potential region of 1.50–3.75 V with a multichannel battery testing system (LAND) at room temperature. Cyclic voltammetry (CV) and electrochemical impedance spectroscopy of the cells were carried out using an electrochemical analyzer (Autolab PGSTAT 302 and CHI 760D potentiostat/galvanostat). In impedance measurements, the frequency range of 100 kHz to 0.01 Hz was used.

Results and discussion

The products were initially characterized by XRD pattern to identify the crystallographic structure and crystallinity. The XRD pattern of $H_2V_3O_8$ (Fig. 1a) shows the formation of an orthorhombic structure (JCPDS No. 01-085-2401). The sharp diffraction peaks imply that the obtained $H_2V_3O_8$ nanowire is well crystallized. The sintered V_3O_7 is a monoclinic structure (Fig. S1, ESI†). This indicates that the phase structure is rebuilt from orthorhombic to monoclinic during the annealing process. In order to confirm the phase transition, thermogravimetric analysis of the $H_2V_3O_8$ nanowire bundles was carried out in a flowing N_2 atmosphere (Fig. 1b). The TG curve shows two steps, which are related to dehydration. The first step up to 125 °C is attributed to the removal of absorbed water on the surface of the product, which can be confirmed by the endothermic peak of the DSC curve. The second step up to 377.5 °C shows the loss of water in the crystal structure, which is corresponding well to the endothermic DSC peak at ~350 °C. The weight lose in this step is 6.1%, and the value is close to the theoretical weight of the
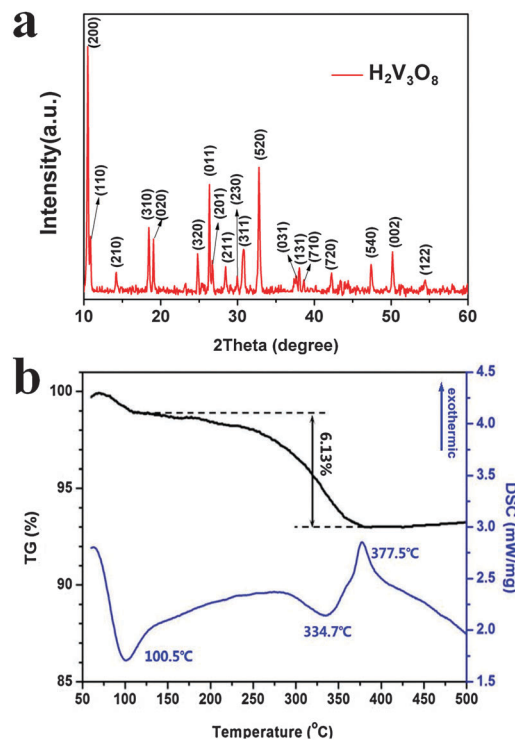

Fig. 1 (a) XRD pattern of $H_2V_3O_8$ nanowires. (b) Thermogravimetric analysis of $H_2V_3O_8$ in N_2.

structural water (6.4%) in $H_2V_3O_8$.[25] There is no weight change from 377.5 °C to 500 °C, which indicates that the water is released completely. While it appears as an exothermic peak in the DSC curve, which has rarely been observed in the previous reports,[19,20] it is confirmed that there is a phase transformation of V_3O_7 to form a more stable structure. There is no obvious boundary between the second endothermic and exothermic peaks, indicating the structure is rebuilt along with the dehydration process.

The structure of $H_2V_3O_8$ is a nearly two-dimensional framework (V_3O_8 layer) comprised of VO_6 octahedra and VO_5 trigonal bipyramids.[26,27] It is very difficult to determine the positions of hydrogen directly, but according to reported results, there are one or two hydrogen atoms firmly attached to a VO_6 octahedron, which makes the hydrogen bonds with the octahedron in the next layer to hold the V_3O_8, giving the three-dimensional structure.[28] When two hydrogen atoms attach, it is thought that the water molecule shares one oxygen atom with VO_6.[20,29] While the unit cell of V_3O_7 is composed of twelve VO_6 octahedra, sixteen VO_5 trigonal bipyramids and eight VO_5 square pyramids, the V_3O_7 is no longer a layered structure.[30]

The morphology and microstructure of the products were investigated by FESEM and TEM. The FESEM images (Fig. 2a and b) reveal that the $H_2V_3O_8$ product is composed of uniform nanowires with a diameter of ~100 nm and a length of several hundred micrometers. Further, many nanowires are almost arranged along the same direction, and form $H_2V_3O_8$ nanowire bundles. After annealing at 400 °C in N_2, the bundled structure still remains (Fig. S2a and b, ESI†). According to the HRTEM (Fig. 2c),
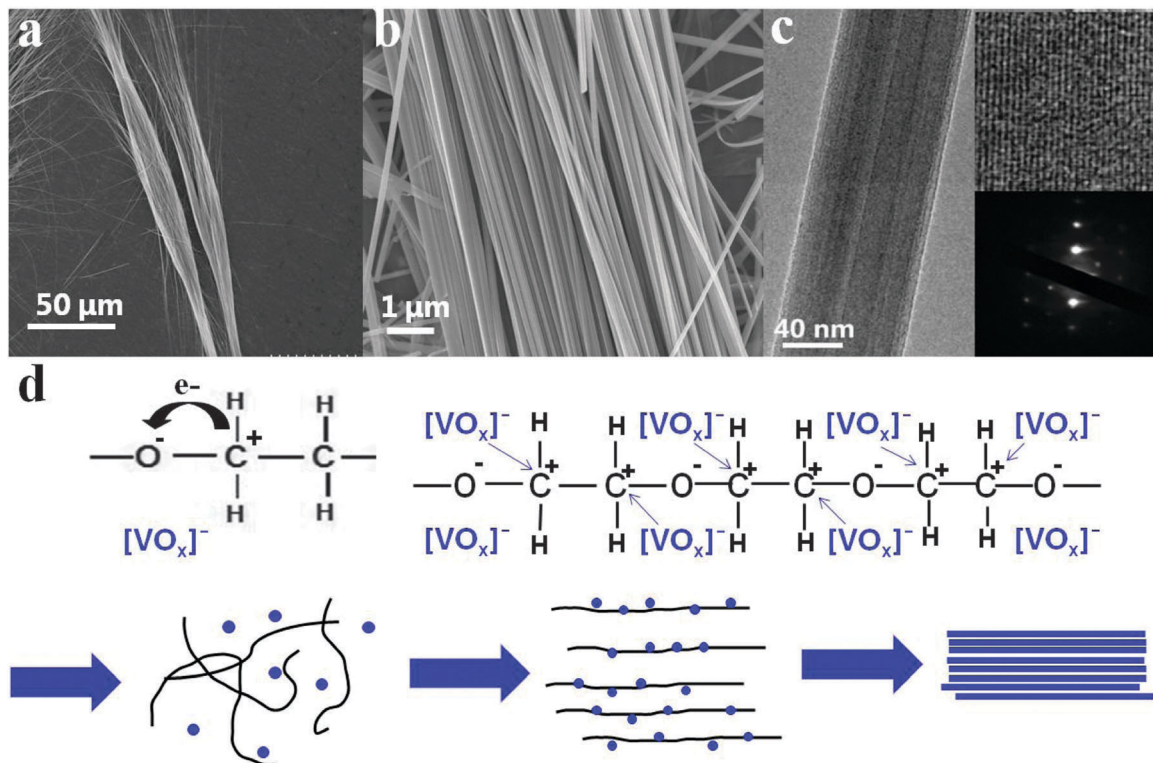
Fig. 2 (a, b) SEM images of the bunched $H_2V_3O_8$ nanowires. (c) TEM, HRTEM (upper inset) images and SAED pattern (lower inset) of $H_2V_3O_8$ nanowires. (d) A schematic illustration of the formation of bunched $H_2V_3O_8$ nanowires.

the lattice fringes of $H_2V_3O_8$ nanowire with regular spacing and the well-resolved fringes confirm the single-crystal nature of the $H_2V_3O_8$ nanowires, which is in accordance with the selected area electron diffraction (SAED) patterns, while the lattice fringes of the V_3O_7 nanowire are not so clear, with lattice defects in the HRTEM image (Fig. S2c, ESI†).

Long chain linear polymer molecules are widely used as a template in synthesizing ultralong nanowires.[31] The polymer template polyethylene glycol (PEG) is reported to play an important role in forming monodirection ultralong nanowires.[32] Ratio-dependent (V_2O_5 sol to PEG) experiments were performed to gain insight into the formation process of such uniform $H_2V_3O_8$ nanowires. Products were collected at different ratios from 4 : 0 to 4 : 2, and their morphologies were examined (Fig. S3, ESI†). When the absence of PEG, the nanowires are only less than ten micrometers with nonhomogeneous diameter, and lay in the random direction. With the increase of PEG, the nanowires become dozens of micrometers long, and also exhibit a bunched morphology. It indicates that PEG is necessary for the quasi-monodirectional structure. In addition, the V_2O_5 powder was also used to replace V_2O_5 sol for reacting with PEG (Fig. S4, ESI†). The length of the obtained nanowires is also up to dozens of micrometers, and the nanowires arrange in random directions. According to these results, we conclude the following growth mechanism in Fig. 2d. Firstly, it is well known that inductive effects universally exist in most polymers, and according to electronegativity theory, the electron clouds will shift to the oxygen atoms in PEG.[28] So the polyoxovanadate clusters with

a negative charge in V_2O_5 sol[33] covered the linear PEG by an electrostatic effect with $C^{\delta+}$. Secondly, the reduction of V_2O_5 was caused by both aniline and PEG, meanwhile the aniline transformed into polyaniline and the PEG was oxidized.[40,41,43,44] The EDS spectrum in Fig. S6 (ESI†) shows that there is no nitrogen in the nanowires, which proves that polyaniline does not exist in the nanowires, and it may be decomposed during the hydrothermal process. Also the EDS spectrum (Fig. S6, ESI†) displays the existence of carbon in the $H_2V_3O_8$ nanowires, indicating that there are some organics remaining in the nanowires, which should derive from the oxidation of PEG. Two absorption peaks at 1390 and 1585 cm^{-1} in the FT-IR spectrum (Fig. S7, ESI†) confirms the presence of –COOH. Thus the redox process may be described as follows.[40]

$$12V_2O_5 + -CH_2CH_2OCH_2CH_2O-$$
$$\rightarrow 8V_3O_7 + -CH_2COOH + -OCH_2COOH + H_2O$$
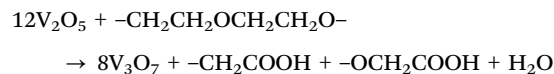
Thirdly, it is well known that the same charges will repel each other,[41,42] so the polyoxovanadate clusters repel each other, and gradually become parallel to each other to reduce the systemic energy. Finally, the ultralong $H_2V_3O_8$ nanowire bundles were synthesized.

Coin cells with metallic lithium as an anode were assembled to investigate the electrochemical performance of the ultralong $H_2V_3O_8$ nanowire cathodes. Cyclic voltammogram (CV) curves of the $H_2V_3O_8$ and V_3O_7 nanowires were measured at a scan rate of 0.1 mV s^{-1} in the potential range from 1.5 to 3.75 V (Fig. 3a).

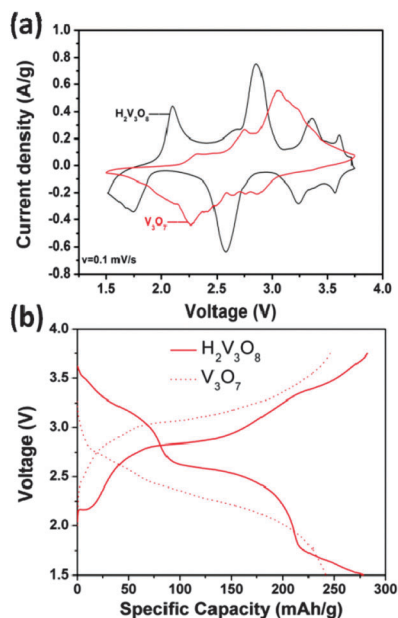Fig. 3 (a) Cyclic voltammogram curves of $H_2V_3O_8$ and V_3O_7 nanowires electrodes at a scanning rate of 0.1 mV s^{-1}. (b) Charge–discharge curves of $H_2V_3O_8$ and V_3O_7 nanowires electrodes at different cycles under 100 mA g^{-1}.

Fig. 4 The cycling performance of $H_2V_3O_8$ and V_3O_7 nanowire electrodes at the current densities of (a) 100 mA g^{-1}, (b) 500 mA g^{-1}, (c) 1000 mA g^{-1}. (d) Cycling performance of the $H_2V_3O_8$ nanowires electrode at the current density of 2000 mA g^{-1}.

The cathodic and anodic peaks are ascribed to the lithium ion insertion and extraction, respectively. For $H_2V_3O_8$ nanowires, four pairs of well defined redox peaks appear at 2.10/1.74, 2.86/2.58, 3.36/3.24 and 3.61/3.57 V, while the main redox peak of V_3O_7 nanowire electrode is observed at 3.06/2.33 V. The charge–discharge voltage profiles of the $H_2V_3O_8$ and V_3O_7 nanowire electrodes at the first cycle are shown in Fig. 3b. It is evident that four plateaus are displayed in the discharge process of the $H_2V_3O_8$ nanowire cathode, while there is only one main plateau in the discharge process of the V_3O_7 nanowire cathode, which agrees well with the CV results.

The cycling performances of the $H_2V_3O_8$ and V_3O_7 nanowires at different current densities of 100–1000 mA g^{-1} are shown in Fig. 4. The initial discharge capacities of $H_2V_3O_8$ and V_3O_7 deliver 278.1 and 241.8 mA h g^{-1} at the current density of 100 mA g^{-1}, respectively. The capacity of the $H_2V_3O_8$ nanowires slightly decays to ~226 mA h g^{-1} in the tenth cycle, and becomes relatively stable in further cycles. This stabilized capacity of $H_2V_3O_8$ nanowires is significantly higher than that of V_3O_7 nanowires. At current densities of 500 and 1000 mA g^{-1}, the discharge capacity only suffers a slight decrease. For example, after 100 cycles, the discharge capacities of $H_2V_3O_8$ and V_3O_7 are found to be 167.8 mA h g^{-1} (93.1% of the initial capacity) and 128.5 mA h g^{-1} (85.2% of the initial capacity) at a current density of 500 mA g^{-1}, respectively. The long-life cycling performance of the $H_2V_3O_8$ nanowires at the high rate is also shown in Fig. 5d. Stable cycling performance is obtained for the rate. After 300 cycles at 2000 mA g^{-1}, 88.0% of the initial capacity (~120 mA h g^{-1}) can be retained, corresponding to the capacity fading of 0.0425% per cycle. However, the V_3O_7 nanowire electrode delivers only an initial discharge capacity of 86.6 mA h g^{-1} (Fig. S5, ESI†). It can be found that the $H_2V_3O_8$
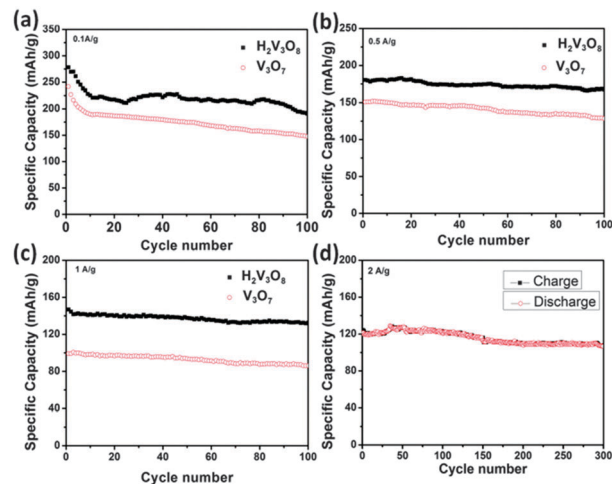
nanowires exhibit the higher capacity and better cycling performance than the V_3O_7 nanowires at different current densities, especially at high current densities.

To evaluate the rate capability, $H_2V_3O_8$ nanowires were cycled at a various charge–discharge rates ranging from 50 to 2000 mA g^{-1} (Fig. 5a). The initial discharge capacity of $H_2V_3O_8$ nanowires can reach as high as 325.7 mA h g^{-1} at the current density of 50 mA g^{-1}, and the inserted Li$^+$ amount (x in Li$_xH_2V_3O_8$) was 3.44, the values are much higher than reported results.[22,27,29] As the current density increases from 100 to 200, 300, 500, 1000, 2000 mA g^{-1}, the discharge capacity decreases gradually from 285.1 to 248.8, 221.8, 197.4, 136.4 and 102.6 mA h g^{-1}, respectively. After the high rate measurement, the current density is returned back to 100 mA g^{-1}, and a discharge capacity of ~245 mA h g^{-1} can be recovered. It can be seen that the $H_2V_3O_8$ nanowires show higher capacity and better rate capability than V_3O_7 nanowires. The electrochemical performances of the ultralong $H_2V_3O_8$ nanowires are comparable to those of many reported $H_2V_3O_8$ electrodes[19,20,22] (Table S1, ESI†).

As we know, the rate capability of an insertion electrode material depends on the kinetics of the lithium ion extraction–insertion process, which is related to the electron transport and lithium ion diffusion length.[34,35] As the rate capability is directly related to the impedance of a cell, the electrochemical impedance spectroscopy (EIS) of $H_2V_3O_8$ and V_3O_7 nanowire electrodes were also measured to provide further insights. The Nyquist plots for $H_2V_3O_8$ and V_3O_7 nanowire electrodes show a straight line in the low frequency region and a depressed semicircle in the high frequency region (Fig. 5b). The size of the semicircle, which shows the charge transfer impedance in the electrode,[36] is clearly smaller for the $H_2V_3O_8$ nanowire electrode. The better connectivity and layered structure of the bundled $H_2V_3O_8$ nanowires may be the main reason for the reduced charge transfer resistance.

To understand the superior performance of $H_2V_3O_8$ nanowires for Li$^+$ storage, we investigated the electrical transport

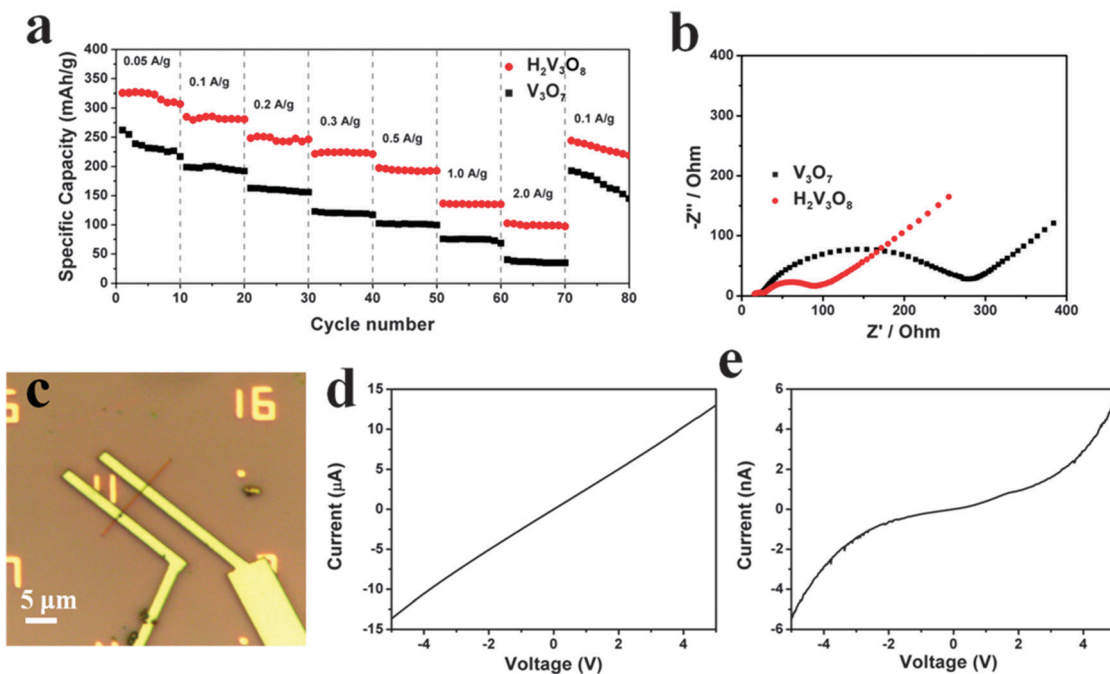**Fig. 5** (a) Rate performances of $H_2V_3O_8$ and V_3O_7 nanowires electrodes. (b) Nyquist plots of $H_2V_3O_8$ and V_3O_7 nanowire electrodes in newly assembled cells. (c) A SEM image of a single nanowire device. Single nanowire transport properties of (d) $H_2V_3O_8$ and (e) V_3O_7 nanowires.

properties through assembling a single nanowire's device before and after annealing (Fig. 5c–e). We deposited vanadium oxide nanowires on a silicon wafer followed by current collector patterning with e-beam lithography and deposition of Cr/Au (10/100 nm) with a thermal evaporator. Before annealing, the I–V characteristics of the nanowire show ohmic behavior (Fig. 5d), and the transported current is in the order of *ca.* 10 μA at 4 V. After annealing, the I–V curve shows asymmetric Schottky barriers (Fig. 5e), and the transported current is of the order of *ca.* 3 nA at 4 V. Therefore, the conductivity of a $H_2V_3O_8$ nanowire increases by close to three orders of magnitude compared to that of the dehydrated nanowire, which indicates the conversion of the $H_2V_3O_8$ nanowire from metallic to semiconductor behaviour during the heat treatment.

The excellent electrochemical performance of ultralong $H_2V_3O_8$ nanowire bundles, especially at high-rate charge and discharge, may be attributed to: (1) the ultralong nanowires offer short distances for Li ion diffusion and a large electrode–electrolyte contact area for rapid Li ion diffusion across the interface, leading to a better rate capability;[9,10,37,38] (2) the ultralong structured nanowires not only provide a long continuous channel for electron transport, but also efficiently reduce the aggregation of the materials.[11] Consequently, they keep their high active surface area, which is favorable for increasing the lithium storage capacity in the electrode; (3) the $H_2V_3O_8$ has a higher electronic conductivity arising from the mixed-valence of V^{4+}/V^{5+};[21,29] (4) The hydrogens linking the V_3O_8 layers provide an elastic buffer space to accommodate the volume expansion/contraction of vanadium layers during the Li insertion–extraction process, thus maintaining the high capacity and good cycling stability.[39]

Conclusions

Ultralong $H_2V_3O_8$ nanowire bundles have been successfully synthesized, and deliver high specific reversible capacity (325.7 mA h g^{-1}) and excellent cycling stability (over 88% capacity retention after 300 cycles at 2000 mA g^{-1}). Compared to V_3O_7 nanowire bundles, ultralong $H_2V_3O_8$ nanowire bundles also exhibit better rate capability. The excellent electrochemical performance of the ultralong $H_2V_3O_8$ nanowire bundle cathode indicates its potential application in high-rate and long-life secondary lithium batteries. It is also demonstrated that our synthesis strategy is facile and versatile for the fabrication of other cathode materials.

Acknowledgements

Notes and references

1 B. Kang and G. Ceder, *Nature*, 2009, **458**, 190.
2 J. M. Tarascon and M. Armand, *Nature*, 2001, **414**, 359.
3 P. Simon and Y. Gogotsi, *Nat. Mater.*, 2008, 7, 845.

4 C. Liu, F. Li, L. P. Ma and H. M. Cheng, *Adv. Mater.*, 2010, **22**, E28.

5 P. G. Bruce, B. Scrosati and J. M. Tarascon, *Angew. Chem., Int. Ed.*, 2008, **47**, 2930.

6 J. Yan, A. Sumboja, E. Khoo and P. S. Lee, *Adv. Mater.*, 2011, **23**, 746.

7 R. Krishnan, T. Ming. Lu and N. Koratkar, *Nano Lett.*, 2011, **11**, 377.

8 H. Zhang, X. D. Yu and P. V. Braun, *Nat. Nanotechnol.*, 2011, **6**, 277.

9 C. K. Chan, H. Peng, G. Liu, K. Mcilwrath, X. F. Zhang, R. A. Huggins and Y. Cui, *Nat. Nanotechnol.*, 2008, **3**, 31.

10 J. Liu, H. Xia, D. F. Xue and L. Lu, *J. Am. Chem. Soc.*, 2009, **131**, 12086.

11 L. Q. Mai, L. Xu, C. H. Han, X. Xu, L. Z. Luo, S. Y. Zhao and Y. L. Zhao, *Nano Lett.*, 2010, **10**, 4750.

12 V. Legagneur, A. Le Gal La Salle, A. Verbaere, Y. Piffard and D. Guyomard, *Electrochim. Acta*, 2002, **47**, 1153.

13 M. S. Whittingham, Y. N. Song, S. Lutta, P. Y. Zavalij and N. A. Chernova, *J. Mater. Chem.*, 2005, **15**, 3362.

14 H. C. Pang, P. Cheng, H. B. Yang, J. L. Lu, C. X. Guo, G. L. Ning and C. M. Li, *Chem. Commun.*, 2013, **49**, 1536.

15 A. Pan, J. G. Zhang, Z. Nie, G. Cao, B. W. Arey, G. Li, S. Q. Liang and J. Liu, *J. Mater. Chem.*, 2010, **20**, 9193.

16 C. Ban, N. A. Chernova and M. S. Whittingham, *Electrochem. Commun.*, 2009, **11**, 522.

17 J. Muster, G. T. Kim, V. Krstić, J. G. Park, Y. W. Park, S. Roth and M. Burghard, *Adv. Mater.*, 2000, **12**, 420.

18 T. Watanabe, Y. Ikeda, T. Ono, M. Hibino, M. Hosoda, K. Sakai and T. Kudo, *Solid State Ionics*, 2002, **151**, 313.

19 H. Q. Li, T. Y. Zhai, P. He, Y. G. Wang, E. Hosonoa and H. S. Zhou, *J. Mater. Chem.*, 2011, **21**, 1780.

20 S. K. Gao, Z. J. Chen, M. D. Wei, K. M. Wei and H. S. Zhou, *Electrochim. Acta*, 2009, **54**, 1115.

21 C. Tsang and A. Manthiram, *J. Electrochem. Soc.*, 1997, **144**, 520.

22 H. Qiao, X. J. Zhu, Z. Zheng, L. Liu and L. Zhang, *Electrochem. Commun.*, 2006, **8**, 21.

23 P. G. Jesús, M. S. Beatriz, A. B. David, M. Emilio, P. F. Juan Carlos, K. Alois and G. A. Flaviano, *J. Power Sources*, 2013, **232**, 173.

24 L. Q. Mai, Y. J. Dong, L. Xu and C. H. Han, *Nano Lett.*, 2010, **10**, 4273.

25 J. Wang, C. J. Curtis, D. L. Schulz and J. G. Zhang, *J. Electrochem. Soc.*, 2004, **151**, A1.

26 Y. Oka, T. Yao and N. Yamamoto, *J. Solid State Chem.*, 1990, **89**, 372.

27 T. Chirayil, P. Y. Zavalij and M. S. Whittingham, *Chem. Mater.*, 1998, **10**, 2629.

28 N. E. Sladek and G. J. Mannering, *Mol. Pharmacol.*, 1969, **5**, 174.

29 Y. Wang and G. Z. Cao, *Chem. Mater.*, 2006, **18**, 2787.

30 C. Li, M. Isobe, H. Ueda, Y. Matsushita and Y. Ueda, *J. Solid State Chem.*, 2009, **182**, 3222.

31 C. V. Subba Reddya, S. Mhoa, R. R. Kalluru and Q. L. Williams, *J. Power Sources*, 2008, **179**, 854.

32 X. Xu, Y. Z. Luo, L. Q. Mai, Y. L. Zhao, Q. Y. An, L. Xu, F. Hu, L. Zhang and Q. J. Zhang, *NPG Asia Mater.*, 2012, **4**, e20.

33 J. Livage, *Chem. Mater.*, 1991, **3**, 578.

34 H. G. Jung, S.-T. Myung, C. S. Yoon, S.-B. Son, K. H. Oh, K. Amine, B. Scrosati and Y.-K. Sun, *Energy Environ. Sci.*, 2011, **4**, 1345.

35 J. Liu, T. E. Conry, X. Y. Song, M. M. Doeff and T. J. Richardson, *Energy Environ. Sci.*, 2011, **4**, 885.

36 R. Ruffo, S. S. Hong, C. K. Chan, R. A. Huggins and Y. Cui, *J. Phys. Chem. C*, 2009, **113**, 11390.

37 T. Y. Zhai, H. M. Liu, H. Q. Li, X. S. Fang, M. Y. Liao, L. Li, H. S. Zhou, Y. Koide, Y. Bando and D. Golberg, *Adv. Mater.*, 2010, **22**, 2547.

38 L. Zhou, D. Y. Zhao and X. W. Lou, *Angew. Chem., Int. Ed.*, 2012, **51**, 239.

39 M. D. Wei, H. Sugihara and I. Honma, *Adv. Mater.*, 2005, **17**, 2964.

40 D. Mantzavinos, E. Lauer, M. Sahibzada, A. Livingston and I. Metcalfe, *Water Res.*, 2000, **34**, 1620.

41 Z. Kang, E. Wang, M. Jiang, S. Lian, Y. Li and C. Hu, *Eur. J. Inorg. Chem.*, 2003, 370.

42 H. Daiguji, P. Yang and A. Majumdar, *Nano Lett.*, 2004, **4**, 137.

43 L. Q. Mai, X. Xu, C. H. Han, Y. Z. Luo, L. Xu, Y. M. Wu and Y. L. Zhao, *Nano Lett.*, 2011, **11**, 4992.

44 L. Q. Mai, Q. L. Wei, Q. Y. An, X. C. Tian, Y. L. Zhao, X. Xu, L. Xu, L. Chang and Q. J. Zhang, *Adv. Mater.*, 2013, **25**, 2969.